Asian Journal of Control, Vol. 19, No. 4, pp. 1–11, July 2017
Published online in Wiley Online Library (wileyonlinelibrary.com) DOI: 10.1002/asjc.1437

IMPROVING ROBUSTNESS FILTER BANDWIDTH IN REPETITIVE CONTROL BY CONSIDERING MODEL MISMATCH

Arnfinn A. Eielsen, Yik R. Teo, and Andrew J. Fleming

ABSTRACT

Repetitive control (RC) is used to track and reject periodic signals by including a model of a periodic signal in the feedback path. The performance of RC can be improved by including an inverse plant response filter, but due to modeling uncertainty at high frequencies, a low-pass robustness filter is also required to limit the bandwidth of the signal model and ensure stability. The design of robustness filters is presently ad-hoc, which may result in excessively conservative performance. This article proposes a new automatic method for designing the robustness filter based on convex optimization and an uncertainty model. Experimental results on a nanopositioning system demonstrate that the proposed method outperforms the traditional brick-wall filter approach.

Key Words: Repetitive control, learning control, uncertainty, optimization.

I. INTRODUCTION

Repetitive control (RC) is a method suited to reference tracking and rejection of periodic signals [1]. The method is based on the internal model principle [2] where an exogenous signal (a reference or disturbance) can be nulled in the error signal if a signal model is contained in the feedback path. RC was developed to reject the periodic disturbances that arise in power supply control [3,4], but has since been used for machining [5], precision positioning [6–8], optical drives [9–11], electro-hydraulics [12], power-converters [13], and scanning probe microscopy [14–16].

Fig. 1 illustrates the signal model used in RC for periodic signals of period L. This implementation is computationally efficient and numerically stable as the model consists of only positive feedback around a time-delay. The corresponding transfer function is an infinite number of marginally stable poles with infinite gain at the harmonics of the periodic reference.

The most common implementation of discrete-time RC was first proposed in [17], where the plant dynamics are inverted using the zero-phase tracking error control (ZPETC) filter in order to improve the RC performance. In principle, an inverse plant response filter (IPRF) should provide a signal model bandwidth up to the Nyquist-frequency. However, the ZPETC filter relies on an accurately identified infinite impulse response (IIR) model, which is not always possible. Furthermore, non-minimum phase zeros cannot be inverted; hence the magnitude response of the ZPETC inverse can be inaccurate.

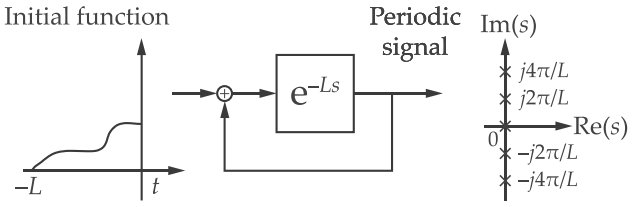

Fig. 1. A time-delay with positive feedback with the appropriate initial function can model any periodic signal [1].

As an alternative to an IIR filter, a finite impulse response (FIR) filter can be used for the IPRF. Compared to a ZPETC inverse, an FIR filter does not require an explicit model structure and can alleviate the problems due to non-minimum phase zeros. However, FIR filters can be more computationally demanding than IIR filters. The IPRF as an FIR filter [18,19] can be found using frequency domain optimization [20]. The foremost difficulties with this approach are the ad-hoc design procedure and non-optimal performance. For example, an error weighting function must be chosen to synthesize a filter which ensures closed-loop stability. An alternative method presented in [8,21] is a more direct method for IPRF synthesis which uses the inverse discrete Fourier transform (IDFT) of the inverse empirical transfer-function estimate (ETFE). This method is

Manuscript received April 13, 2016; revised August 4, 2016; accepted October 10 2016.

All authors are with the Precision Mechatronics Labs at the School of Electrical Engineering and Computer Science, The University of Newcastle, 2308 Callaghan, New South Wales, Australia.

Yik Teo is the corresponding author (e-mail: yik.teo@newcastle.edu.au).

equivalent to the frequency sampling method for FIR filter synthesis [22].

The performance and stability of RC depends on the accuracy of the IPRF, regardless of whether the implementation is an IIR or FIR filter. The robustness and stability of the closed-loop system is related to the magnitude of modeling errors. A simple method for achieving robustness is to limit the bandwidth using a low-pass filter [1,23–27], or truncating the number of poles in the signal model [28]. A low-pass robustness filter [24,25] improves the stability margin at higher frequencies, where the plant mismatch is greatest.

In this article, a new method is proposed for synthesizing a robustness filter based on the magnitude of modeling uncertainty. This approach is shown to be less conservative than present methods and is demonstrated to improve the tracking performance of an experimental nanopositioning system.

II. DISCRETE-TIME REPETITIVE CONTROL

Fig. 2 shows a block diagram for a general RC scheme applied to a plant $G(z^{-1})$. The filters $H_1(z^{-1})$ and $H_2(z^{-1})$ are used to produce a bandwidth-limited signal generator. The filter $H_1(z^{-1})$ is known as the robustness filter [24,25]. If $H_1(z^{-1})$ and $H_2(z^{-1})$ have linear phase, and therefore constant group delay, then a group delay of L will produce poles at $\pm j2\pi n/L$, $n \in \mathbb{N}_0$, where $\mathbb{N}_0$ denotes the set of natural numbers including zero. Symmetric FIR filters have a linear phase response; which is why, ideally, $H_1(z^{-1})$ and $H_2(z^{-1})$ are chosen to be such filters. The magnitude response of $H_1(z^{-1})$ and $H_2(z^{-1})$ can then be used to limit the closed-loop bandwidth. The IPRF $H_3(z^{-1})$ can be implemented as either an IIR or FIR filter.

In Fig. 2 the RC scheme can be seen as equivalent to the control law

$$C_{RC}(z^{-1}) = \frac{H_1(z^{-1})H_3(z^{-1})}{1 - H_1(z^{-1})H_2(z^{-1})}. \tag{1}$$

Assuming that the reference signal period is an integer multiple of the sampling time T_s, then the product of $H_1(z^{-1})H_2(z^{-1})$ in the denominator has to contain a delay of z^{-N}, where

$$N = L/T_s, \tag{2}$$

to satisfy the internal model principle.

The closed-loop sensitivity function is

$$\begin{aligned} S(z^{-1}) &= \frac{E(z^{-1})}{R(z^{-1})}, \\ &= \frac{1 - H_1(z^{-1})H_2(z^{-1})}{1 - H_1(z^{-1})\left(H_2(z^{-1}) - H_3(z^{-1})G(z^{-1})\right)}, \end{aligned} \tag{3}$$

which can be rearranged to the form shown in Fig. 3. The stability of the RC system is determined by the denominator of (3), which will provide stability if the loop transfer-function in Fig. 3 satisfies the small-gain theorem [24,25]. Therefore, the system is stable if

$$\left\| H_1(z^{-1})\left(H_2(z^{-1}) - H_3(z^{-1})G(z^{-1})\right)\right\|_\infty < 1, \tag{4}$$

assuming $H_1(z^{-1})$ and $H_2(z^{-1})$ are stable. The stability condition can be split into two conditions:

$$\left\| H_1(z^{-1})\right\|_\infty \leq 1, \tag{5}$$

and

$$\left\| H_2(z^{-1}) - H_3(z^{-1})G(z^{-1})\right\|_\infty < 1. \tag{6}$$

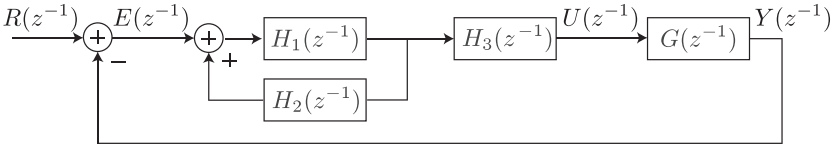

Fig. 2. Block diagram for a general RC system.

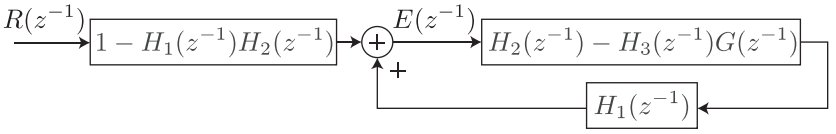

Fig. 3. Equivalent description of sensitivity function.

III. THE INVERSE PLANT RESPONSE FILTER

The IPRF can be implemented by a model-less FIR filter [8,21]. This method relies on an empirical transfer-function estimate (ETFE) [29] of the plant. The frequency sampling method for filter synthesis and Welch's method for estimating the ETFE are described in the following subsections.

3.1 Synthesizing the inverse plant response filter

In terms of the frequency samples $k \in [0, M-1] \cap \mathbb{N}_0$, the ETFE of the plant is denoted $\hat{G}(k)$, and its inverse is denoted $\hat{G}^{-1}(k)$. The IPRF $H_3(z)$ is an FIR filter that can be found by taking the inverse discrete Fourier transform (IDFT) of $\hat{G}^{-1}(k)$. This method is known as the frequency-sampling method for FIR filter synthesis [22]. The unit impulse response $g_i(n)$ of the inverse of the ETFE $\hat{G}^{-1}(k)$ is

$$g_i(n) = \frac{1}{M} \sum_{k=0}^{M-1} \hat{G}^{-1}(k) \mathrm{e}^{j\frac{2\pi kn}{M}} , \tag{7}$$

where $n \in [0, M-1] \cap \mathbb{N}_0$. The IDFT is found in MATLAB using the function `ifft`. The FIR filter is then expressed in the z-domain as

$$\begin{aligned} F(z^{-1}) &= g_i(0) + g_i(1)z^{-1} + \ldots + g_i(M-1)z^{-M+1} \\ &= \sum_{n=0}^{M-1} g_i(n) z^{-n} . \end{aligned} \tag{8}$$

The frequency-sampling method results in a unit impulse response which has been convoluted with a rectangular window of the same length in the frequency domain. The frequency response of $F(z^{-1})$ is therefore affected by the large side-lobes of the rectangular window. As a result, the modeling error of $F(z^{-1})$ is large between the frequency samples. This can be alleviated by the use of a window function with smaller side-lobes, which effectively smooths the frequency response of $F(z^{-1})$.

A windowed FIR filter $\tilde{h}(n)$ is created from an FIR filter $h(n)$ as

$$\tilde{h}(n) = w(n)h(n) \tag{9}$$

where $w(n)$ is a window function that is non-zero only for $n \in [0, M-1] \cap \mathbb{N}_0$. The frequency-domain representation of the window function $W(k)$ is

$$\begin{aligned} W(k) &= \sum_{n=0}^{M-1} w(n - M/2) \mathrm{e}^{-j\frac{2\pi kn}{M}} \\ &= \left[\sum_{n=0}^{M-1} w(n) \mathrm{e}^{-j\frac{2\pi kn}{M}} \right] \mathrm{e}^{-j\frac{2\pi k}{M}\frac{M}{2}} , \end{aligned} \tag{10}$$

where the term $\mathrm{e}^{-j(2\pi k/M)(M/2)}$ comes from the fact that the rectangular window is not centered around $n = 0$, but is time-shifted to be centered around $n = M/2$. This phase term will cause distortion of $h(n)$, unless $h(n)$ is also phase-shifted to compensate. The unit impulse response $g_i(n)$ is therefore phase-shifted before windowing. Due to the circular shift property of the discrete Fourier transform (DFT), this can be done by rearranging $g_i(n)$ such that

$$\bar{g}_i(n) = \begin{cases} g_i(n + M/2) , & n = 0, 1, \ldots, \frac{M}{2} - 1 \\ g_i(n - M/2) , & n = \frac{M}{2}, \frac{M}{2} + 1, \ldots, M-1 \end{cases} \tag{11}$$

for the case when M is even. The inverse response is then represented by the FIR filter

$$\bar{F}(z^{-1}) = \sum_{n=0}^{M-1} \bar{g}_i(n) z^{-n} = z^{-M/2} F(z^{-1}) \tag{12}$$

which is $F(z^{-1})$ delayed by $M/2$ steps. Applying the window $w(n)$ to the time-shifted impulse response $\bar{g}_i(n)$,

$$\tilde{g}_i(n) = w(n)\bar{g}_i(n) , \tag{13}$$

the filter

$$\tilde{F}(z^{-1}) = W(z^{-1}) * \left[z^{-M/2} F(z^{-1}) \right] \tag{14}$$

is obtained, and $H_3(z^{-1}) = \tilde{F}(z^{-1})$ is used in (1).

For the implementation, $M = N$, assuming N to be even, and the stability condition given in (6) is simplified by choosing

$$H_2(z^{-1}) = z^{-N/2} , \tag{15}$$

since $|H_2(z^{-1})| = 1$, which results in

$$\begin{aligned} &\left\| z^{-N/2} - z^{-N/2} \left[F(z^{-1}) * W(z^{-1}) \right] G(z^{-1}) \right\|_\infty \\ &= \left\| 1 - \left[W(z^{-1}) * F(z^{-1}) \right] G(z^{-1}) \right\|_\infty < 1 , \end{aligned} \tag{16}$$

where $\left[W(z^{-1}) * F(z^{-1}) \right] G(z^{-1}) \approx 1$ if the FIR filter inverse is accurate.

3.2 Empirical transfer-function estimate

To obtain an accurate empirical transfer-function estimate (ETFE), several methods can be used, including periodic averaging, and Welch's averaged periodogram [21,29].

Welch's method [30] is one of the most common methods for obtaining an ETFE for RC [18,19,31]. The plant output data is usually generated using Gaussian white-noise excitation, although more informative input signals can be generated by experiment design, if prior information about the plant is known [29,32,33]. The ETFE of the plant $\hat{G}(k)$, and its inverse $\hat{G}^{-1}(k)$, are found as the quotient of the cross power spectral density estimate of the input and the measured output $P_{yu}(k)$, and the power spectral density estimate of the input $P_{uu}(k)$, *i.e.*,

$$\hat{G}(k) = \frac{P_{yu}(k)}{P_{uu}(k)}\,, \text{ and } \hat{G}^{-1}(k) = \frac{P_{uu}(k)}{P_{yu}(k)}\,.$$

In Welch's method, the time-series data is divided into windowed segments, with an option to use overlapping segments. Then, a modified periodogram of each segment is computed and the results are averaged [30]. Welch's method for generating an ETFE corresponds to the function `tfestimate` in MATLAB. One of the advantages of Welch's method is the flexibility in terms of the number of frequency samples and excitation signal used.

IV. THE ROBUSTNESS FILTER

The performance and stability of RC depends on the accuracy of the IPRF $H_3(z^{-1})$, which typically deteriorates at higher frequencies. The stability and robustness of the system is improved by limiting the RC gain by way of the robustness filter $H_1(z^{-1})$ [25]. This is commonly done using a low-pass filter, increasing the attenuation at higher frequencies, thus reducing the bandwidth [24]. In this Section, a novel method for synthesizing an FIR robustness filter is presented.

4.1 Synthesizing the robustness filter

There are two requirements for the robustness filter. The product of the filters $H_1(z^{-1})$ and $H_2(z^{-1})$ should produce a delay of N, and the stability condition (5) must be met. Linear phase is ensured by using a symmetric FIR filter. The required delay in (2) is ensured by using a filter with $2P+1$ taps, with

$$P = N/2\,, \tag{17}$$

assuming N is even. This filter will have $P+1$ unique parameters. In addition, a desired magnitude response $\left|H_1(\omega)\right|$ is specified as part of the control law design. By pre-multiplying the filter by z^P, $H_1(z^{-1})$ can be expressed as the non-causal, zero-phase filter

$$\begin{aligned}\bar{H}_1(z^{-1}) = {} & h_1(P)z^P + h_1(P-1)z^{P-1} + \ldots \\ & + h_1(0) + \ldots + h_1(P-1)z^{-P+1} + h_1(P)z^{-P}\,.\end{aligned} \tag{18}$$

Since $z = \mathrm{e}^{j\omega}$ and $\mathrm{e}^{jn\omega} + \mathrm{e}^{-jn\omega} = 2\cos(n\omega)$, the frequency response is real-valued and found as

$$\bar{H}_1(\omega) = h_1(0) + 2\sum_{n=1}^{P}\cos(n\omega)h_1(n) = \left|H_1(\omega)\right|\,. \tag{19}$$

Consider $m_f \geq P+1$ frequency samples $\omega_k \in [0, \pi]$, since the spectrum of $\left|H_1(\omega)\right|$ is symmetric, then the response can be expressed as

$$\mathbf{A}_{\bar{H}_1} = \mathbf{\Omega}\mathbf{\Theta}_{h_1} \tag{20}$$

where

$$\mathbf{A}_{\bar{H}_1} = \begin{bmatrix} |H_1(\omega_1)| & \cdots & |H_1(\omega_{m_f})| \end{bmatrix}^{\mathrm{T}}, \tag{21}$$

$$\mathbf{\Omega} = \begin{bmatrix} \mathbf{\Omega}_1 \\ \vdots \\ \mathbf{\Omega}_{m_f} \end{bmatrix}, \tag{22}$$

$$\mathbf{\Omega}_i = \begin{bmatrix} 1 & 2\cos(\omega_i) & \cdots & 2\cos(P\omega_i) \end{bmatrix}, \tag{23}$$

and

$$\mathbf{\Theta}_{h_1} = \begin{bmatrix} h_1(0) & h_1(1) & \cdots & h_1(P) \end{bmatrix}^{\mathrm{T}}. \tag{24}$$

The coefficients that approximate the desired magnitude response for the robustness filter $\left|H_1(\omega)\right|$, that ensure a linear-phase and $|H_1(\omega)| \leq 1$, can be found solving the convex optimization problem [34]

$$\begin{aligned} &\underset{\Theta}{\text{minimize}} \;\; \|\mathbf{\Omega}\mathbf{\Theta}_{h_1} - \mathbf{A}_{\bar{H}_1}\|_2 \\ &\text{s.t.} \;\; \mathbf{\Omega}\mathbf{\Theta}_{h_1} \leq \mathbf{1}, \end{aligned} \tag{25}$$

where $\mathbf{1}$ denotes a column vector of ones, and time-shifting the resulting filter

$$H_1(z^{-1}) = z^{-P}\bar{H}_1(z^{-1})\,. \tag{26}$$

When solving this problem, a sufficient number of frequency samples are necessary to avoid an under-determined problem. To improve the inter-sample response of the resulting filter [20,35], a higher number of samples is usually required, hence

$$m_f = 10\,(P+1)$$

was used for the results in this paper.

4.2 Brick-wall low-pass filter approach

A linear-phase low-pass filter approximating a brick-wall frequency response is the most common method of designing the robustness filter $H_1(z^{-1})$ [1,23–27]. Approximating the ideal step-function using an FIR filter typically introduces pass-band ripple [20,22], which causes the stability condition (5) to be violated. One way to practically eliminate pass-band ripple is to approximate the brick-wall frequency response using the magnitude response of a high-order low-pass Butterworth filter. The roll-off rate of the Butterworth is also lower than more direct step-function approximations, which should lead to a less severe bandwidth limitation. The bandwidth of the filter is chosen to be the frequency domain where $|H_3(z^{-1})\hat{G}(z^{-1})| \approx 1$, where $\hat{G}(z^{-1})$ is the ETFE of the plant $G(z^{-1})$.

4.3 Mismatch approach

When evaluating the mismatch between the measured response and the IPRF, it is often apparent that a brick-wall filter is more conservative than necessary. By considering the mismatch when synthesizing the robustness filter $H_1(z^{-1})$, a less conservative filter can be obtained. Here, the robustness filter problem is solved as an optimization problem taking the measured uncertainty, or model mismatch, into consideration.

The stability criterion (4) can be written:

$$\left|H_1(z^{-1})\left(H_2(z^{-1}) - H_3(z^{-1})G(z^{-1})\right)\right| \leq 1\,. \tag{27}$$

If the model mismatch is denoted as

$$\delta(z^{-1}) = z^{N/2}H_3(z^{-1})G(z^{-1}) \tag{28}$$

the stability criterion is

$$\begin{aligned}&\left|H_1(z^{-1})\left(z^{-N/2} - z^{-N/2}\delta(z^{-1})\right)\right| \\ &= \left|H_1(z^{-1})\left(1 - \delta(z^{-1})\right)\right| = \left|H_1(z^{-1})\upsilon(z^{-1})\right| \leq 1\,,\end{aligned} \tag{29}$$

where the mismatch is expressed by way of the multiplicative uncertainty weight

$$\upsilon(\omega) = \delta(\omega) - 1\,. \tag{30}$$

A design criterion for $H_1(z^{-1})$ can then be found as:

$$\left|H_1(\omega)\right| \leq \frac{1}{|\upsilon(\omega)|} \tag{31}$$

There are two main contributors to model mismatch. First, assume a perfect ETFE $\hat{G}(k) = G(k)$ and corresponding inverse FIR filter $F(z^{-1})$; the required windowing $W(z^{-1})$ introduces a modeling error in the IPRF $H_3(z^{-1}) = z^{-N/2}\left[W(z^{-1}) * F(z^{-1})\right]$ since

$$\left[W(z^{-1}) * F(z^{-1})\right] G(z^{-1}) \neq 1\,.$$

Second, the ETFE can not be expected to be perfectly accurate, due to non-linearity, noise, and other factors influencing the dynamics of the actual system.

4.3.1 Measuring the Model Mismatch

The method adopted here in order to measure the model uncertainty, is to produce a more accurate, higher resolution ETFE $\hat{G}_m(k)$ than the EFTE $\hat{G}(k)$ used to generate the IPRF, and then compute the measured uncertainty weight

$$\upsilon_m(k) = \left[W(k) * F(k)\right]\hat{G}_m(k) - 1\,, \tag{32}$$

that can be used to generate the uncertainty bound, described in Sec. 4.4.

The reason for using a higher frequency resolution ETFE is that in the spectral density estimates used to generate the ETFE, the frequency bins represent average power, and hence the power due to large peaks in the amplitude response can be spread over a wide frequency domain if the frequency resolution is low. This reduces the observed maximum gain, and can therefore lead to an underestimation of the model mismatch. The remedy is to use a high frequency resolution; increasing the resolution until no significant increase in the peaks of the ETFE is observed.

4.4 Approximating the measured uncertainty

The measured uncertainty can not be expected to capture all the uncertainty present in the system. It is therefore necessary to compute a more conservative estimate $\hat{\upsilon}(z^{-1})$ of the uncertainty; over-bounding the measured uncertainty. One way to achieve this is to consider the positive-real rational function

$$\hat{\Upsilon}(z^{-1}) = \frac{\hat{\Upsilon}_b(z^{-1})}{\hat{\Upsilon}_a(z^{-1})} \triangleq \hat{\upsilon}(z^{-1})\hat{\upsilon}(z) = |\hat{\upsilon}(\omega)|^2 \tag{33}$$

with order Q, where

$$\begin{aligned}\hat{\Upsilon}_b(z^{-1}) = {} & b(Q)z^{Q} + b(Q-1)z^{Q-1} + \dots \\ & + b(0) + \dots + b(Q-1)z^{-Q+1} + b(Q)z^{-Q}\,.\end{aligned} \tag{34}$$

and

$$\hat{\Upsilon}_a(z^{-1}) = z^Q + a(Q-1)z^{Q-1} + \dots + a(0) + \dots + a(Q-1)z^{-Q+1} + z^{-Q}. \quad (35)$$

Here, $a(Q) = 1$, and the rational function has $2Q+1$ unique coefficients. The frequency response is

$$\hat{\Upsilon}(\omega) = \frac{b(0) + 2\sum_{n=1}^{Q}\cos(n\omega)b(n)}{a(0) + 2\sum_{n=1}^{Q-1}\cos(n\omega)a(n) + 2\cos(Q\omega)}, \quad (36)$$

and for $n_f \geq 2Q+1$ frequency samples, *i.e.* the number of samples used to compute (32), $\omega_i \in [0, \pi]$ it can be expressed as

$$\left[\, \boldsymbol{\Omega}, -\boldsymbol{\Omega}_{\mathbf{A}_{\upsilon_m}} \,\right] \begin{bmatrix} \boldsymbol{\Theta}_b \\ \boldsymbol{\Theta}_a \end{bmatrix} = \boldsymbol{\omega}_Q \circ \mathbf{A}_{\upsilon_m} \quad (37)$$

where $\circ$ denotes the Hadamard product, and

$$\mathbf{A}_{\upsilon_m} = \left[\, |\upsilon_m(\omega_1)|^2 \;\cdots\; |\upsilon_m(\omega_{n_f})|^2 \,\right]^{\mathrm{T}}, \quad (38)$$

$$\boldsymbol{\Omega} = \begin{bmatrix} \boldsymbol{\Omega}_1 \\ \vdots \\ \boldsymbol{\Omega}_{n_f} \end{bmatrix}, \quad (39)$$

$$\boldsymbol{\Omega}_i = \left[\, 1 \;\; 2\cos(\omega_i) \;\cdots\; 2\cos(Q\omega_i) \,\right], \quad (40)$$

$$\boldsymbol{\Omega}_{\mathbf{A}_\upsilon} = \bar{\boldsymbol{\Omega}} \circ \left(\mathbf{A}_\upsilon \otimes \mathbf{1}^{\mathrm{T}} \right) \quad (41)$$

$$\bar{\boldsymbol{\Omega}} = \begin{bmatrix} \bar{\boldsymbol{\Omega}}_1 \\ \vdots \\ \bar{\boldsymbol{\Omega}}_{n_f} \end{bmatrix}, \quad (42)$$

$$\bar{\boldsymbol{\Omega}}_i = \left[\, 1 \;\; 2\cos(\omega_i) \;\cdots\; 2\cos((Q-1)\omega_i) \,\right], \quad (43)$$

$$\boldsymbol{\omega}_Q = \left[\, 2\cos(Q\omega_1) \;\cdots\; 2\cos(Q\omega_{n_f}) \,\right]^{\mathrm{T}}, \quad (44)$$

$$\boldsymbol{\Theta}_b = \left[\, b(0) \;\; b(1) \;\cdots\; b(Q) \,\right]^{\mathrm{T}}, \quad (45)$$

$$\boldsymbol{\Theta}_a = \left[\, a(0) \;\; a(1) \;\cdots\; a(Q-1) \,\right]^{\mathrm{T}}, \quad (46)$$

where $\otimes$ denotes the Kronecker product.

Using a positive-real rational function makes it possible to solve for an over-bounding interpolation $\Upsilon(z^{-1})$ using convex optimization [34]:

$$\begin{aligned} \underset{\Theta}{\text{minimize}} \;\; & \|\mathbf{X}\boldsymbol{\Theta} - \mathbf{Y}\|_1 \quad (47) \\ \text{s.t.} \;\; & \mathbf{X}\boldsymbol{\Theta} - \mathbf{Y} \geq \mathbf{0} \\ & \boldsymbol{\Omega}\boldsymbol{\Theta}_b \geq \gamma_b \mathbf{1} \\ & \boldsymbol{\Omega} \left[\boldsymbol{\Theta}_a{}^{\mathrm{T}} \;\; 1 \right]^{\mathrm{T}} \geq \gamma_a \mathbf{1} \end{aligned}$$

where

$$\mathbf{X} = \left[\, \boldsymbol{\Omega}, -\boldsymbol{\Omega}_{\mathbf{A}_\upsilon} \,\right], \; \boldsymbol{\Theta} = \begin{bmatrix} \boldsymbol{\Theta}_b \\ \boldsymbol{\Theta}_a \end{bmatrix}, \text{ and } \mathbf{Y} = \boldsymbol{\omega}_Q \circ \mathbf{A}_\upsilon .$$

If $\gamma_a, \gamma_b \geq 0$, the constraints ensure that both the numerator and denominator will be positive-real. The first constraint ensures the over-bound. The values of γ_a and γ_b can be used to control the slope of the interpolation, by reducing the depths and peaks of the zeros and poles. A stable transfer-function weight $\hat{\upsilon}(z^{-1})$ can also be obtained by spectral factorization of $\hat{\Upsilon}(z^{-1}) = \hat{\upsilon}(z^{-1})\hat{\upsilon}(z)$. The desired magnitude response for $H_1(z^{-1})$ can then be computed from

$$\left| H_1(\omega) \right| \leq \frac{1}{k_s \left| \hat{\upsilon}(\omega) \right|}, \quad (48)$$

where the constant $k_s \geq 1$ has been introduced to provide an additional stability margin, to account for any unmeasured and unknown effects.

V. EXPERIMENTAL RESULTS

5.1 System description

The experiments were conducted on the two-axis serial-kinematic nanopositioning stage shown in Fig. 4. Each axis contains a 12μmm long piezoelectric stack actuator (Noliac NAC2003-H12) with a free displacement of 12 µm at 200 V. The flexure design includes a mechanical amplifier to provide a total range of 30 µm. The flexures also mitigate cross-coupling such that each axis can be controlled independently. More details on the design of this stage can be found in [36]. The displacement of the moving platform is measured by a Microsense 6810 capacitive gauge and 6504-01 probe, which has a sensitivity of 2.5µm/V. The stage is driven a by PiezoDrive PDL200 voltage amplifier with a gain of 20 V/V. The control law was implemented on a dSPACE DS1104 hardware-in-the-loop system via Simulink Coder. The anti-aliasing and reconstruction filters were implemented using two Stanford Research System SIM965 analog filters. The experiments were done using the x-axis. The sampling frequency of the system was 10kHz and the reference was a 40-Hz triangle wave, *i.e.*, $T_s = 0.1$ ms and $L = 25$ ms which resulted in $N = 250$.

5.2 Inverse plant response filter

The IPRF $H_3(z^{-1})$ is an FIR filter synthesized using frequency sampling, as discussed in Sec. 3.1. A Hann window was applied to the FIR filter to improve the inter-sample response. Welch's method, discussed in Sec. 3.2, with $N = 250$ frequency samples and a Hamming window was used to generate the ETFE. In Fig. 5, the frequency response of the ETFE and FIR inverse filter $H_3(z^{-1})$ is plotted, as well as the product $z^{N/2}H_3(z^{-1})\hat{G}(z^{-1})$, where $\hat{G}(z^{-1})$ is the ETFE with $N = 250$ frequency samples.

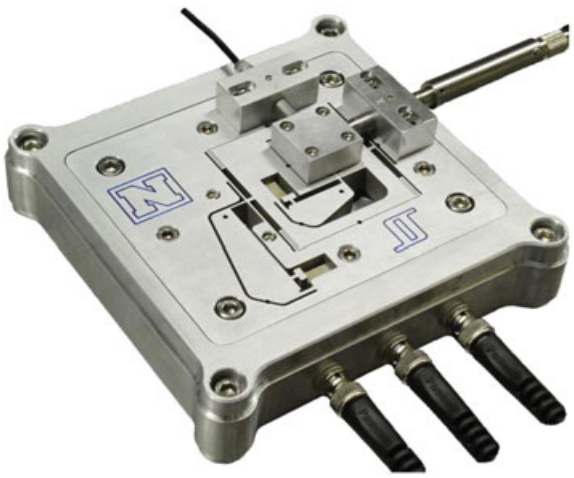

Fig. 4. Two-axis serial-kinematic nano-positioning platform [36].

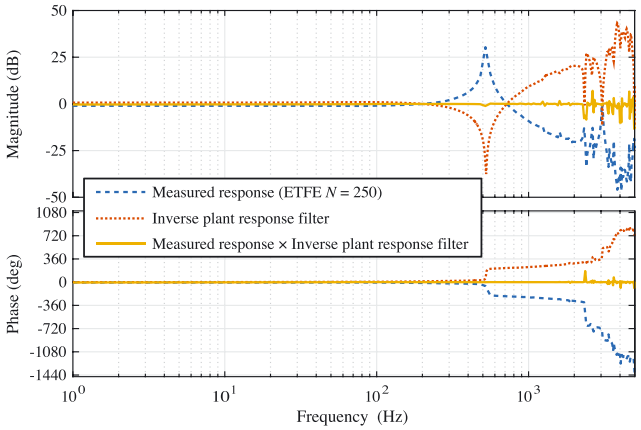

Fig. 5. ETFE, IPRF, and the product of the ETFE and IPRF.

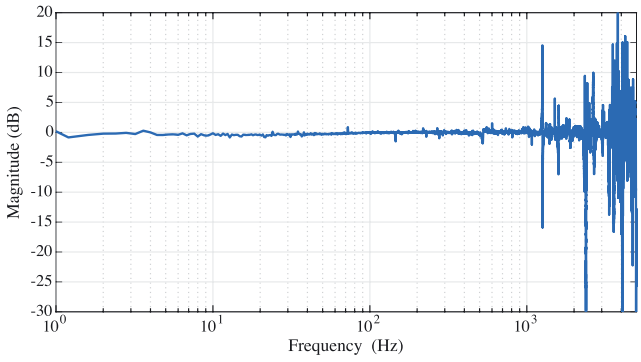

Fig. 6. The magnitude of the model mismatch (28); the product between the high resolution empirical transfer-function estimate (ETFE) and the inverse plant response filter (IPRF).

5.3 Brick-wall low-pass filter approach

The number of taps in $H_3(z^{-1})$ is dictated by (2). The number of taps limits the frequency resolution of the filter, and the Hann window used to improve the inter-sample behavior of the $H_3(z^{-1})$ also reduces the accuracy of the model at the frequency samples. Hence, there will be a mismatch between the IPRF and the plant response. A high-resolution ETFE with 25 000 frequency samples was generated using Welch's method in order to produce a good estimate of the mismatch. The measured mismatch is shown in Fig. 6, where the $|H_3(z^{-1})\hat{G}(z^{-1})|$ is shown to be approximately unity up to about 1.25 kHz.

The desired magnitude response $|H_1(z^{-1})|$ of the filter was chosen to be the magnitude response of a 24th-order low-pass Butterworth filter with a cut-off frequency of 1.15 kHz that was discretized using zero-order hold. The frequency response of the filter and the stability criterion (4) are plotted in Fig. 7.

5.4 Mismatch approach

In Fig. 8, the relative error (30) of the system is shown. The uncertainty between the high resolution ETFE and the IPRF is large at higher frequency. The magnitude response of $\hat{v}(z^{-1})$ is the uncertainty bound of the system represented by the dashed line. This bound was found using the method in Sec. 4.4, where $Q = 11$, $\gamma_a = 5$ and $\gamma_b = 100$. The stability margin of the system is increased by using $k_s = 1.5$. Due to the hysteresis in the piezoelectric actuator, the effective gain of the actuator is known to change by up to 80% [37], hence a constant margin should capture this uncertainty well. The frequency response of the filter and the stability criterion (4) are shown in Fig. 9.

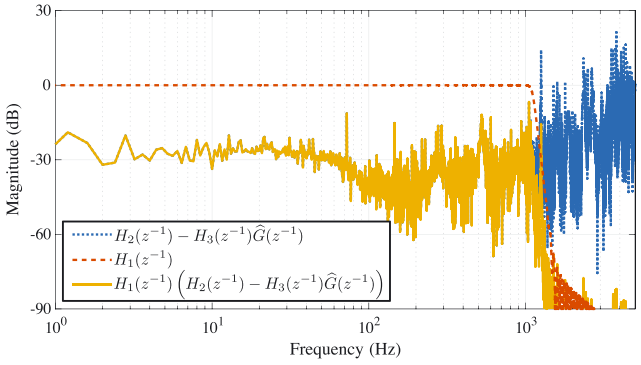

Fig. 7. Robustness filter $H_1(z^{-1})$ and stability criterion (brick-wall).

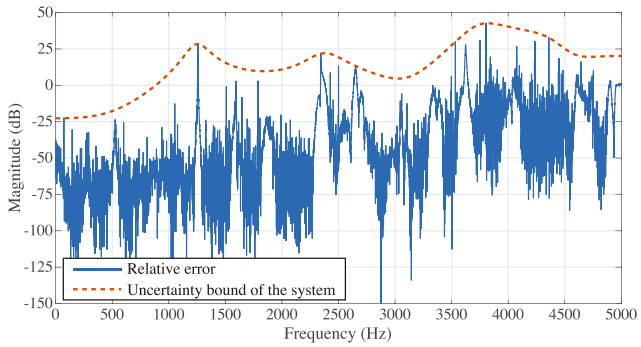

Fig. 8. Relative model mismatch (30) and estimated uncertainty over-bound $\hat{v}(z^{-1})$ for the system.

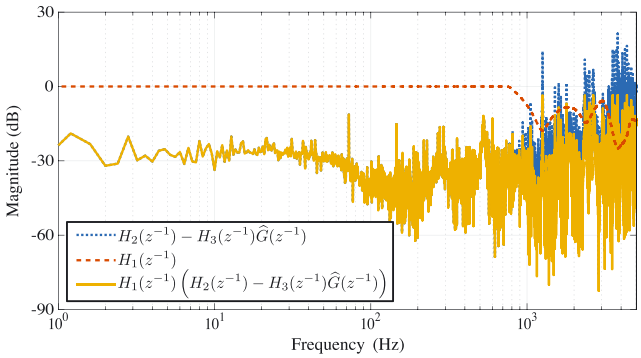

Fig. 9. Robustness filter $H_1(z^{-1})$ and stability criterion (mismatch).

VI. RESULTS

The reference signal is a ±5 μm triangular wave at 40 Hz. The reference signal and the measured steady-state displacement for both RC configurations is shown in Fig. 10. The absolute value of the steady-state error signal is shown in Fig. 11. With y as the measured output and r as the reference, the error signal is denoted $e = r - y$. The maximum tracking error (ME) is then defined as

$$e_{\max}\,(\%) = \frac{\max|e|}{\max y - \min y} \times 100\%\,,$$

and the normalized root-mean-squared error (NRSME) is defined as

$$e_{\mathrm{RMS}}\,(\%) = \frac{\sqrt{\frac{1}{N}\sum_{n=0}^{N-1}|e(n)|^2}}{\max y - \min y} \times 100\%\,.$$

The tracking performance results are summarized in Tab. I.

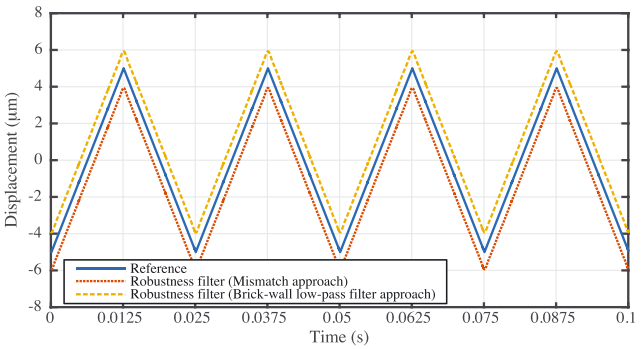

Fig. 10. Measured displacements, offset by ±1 μm to enhance viewing.

Table I. Tracking error for a ±5 μm triangle wave at 40 Hz.

Robustness filter design	$e_{\max}$ (%)	e_{RMS} (%)
Brick-wall low-pass filter approach	0.7904	0.0902
Mismatch approach	0.7217	0.0856

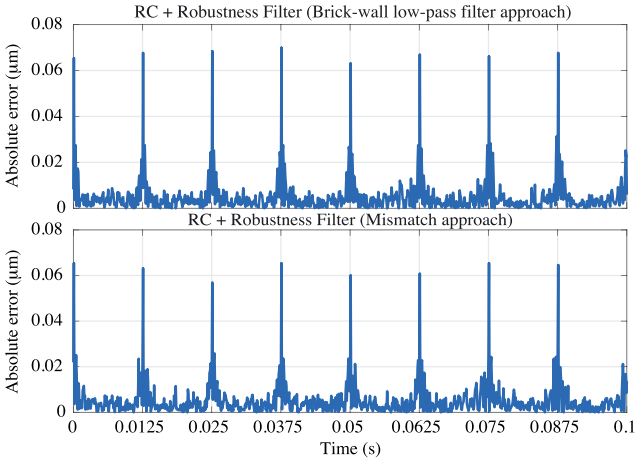

Fig. 11. The absolute value of the displacement error.

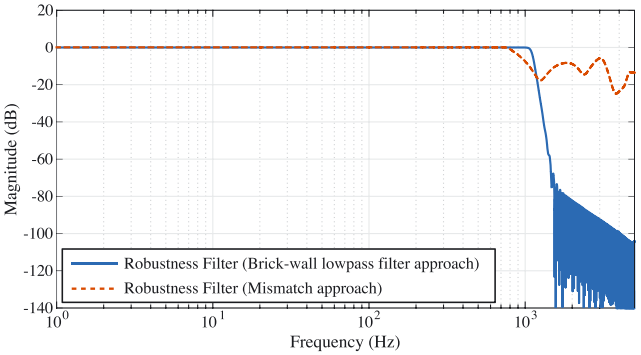

Fig. 12. Comparison of the robustness filters $H_1(z^{-1})$.

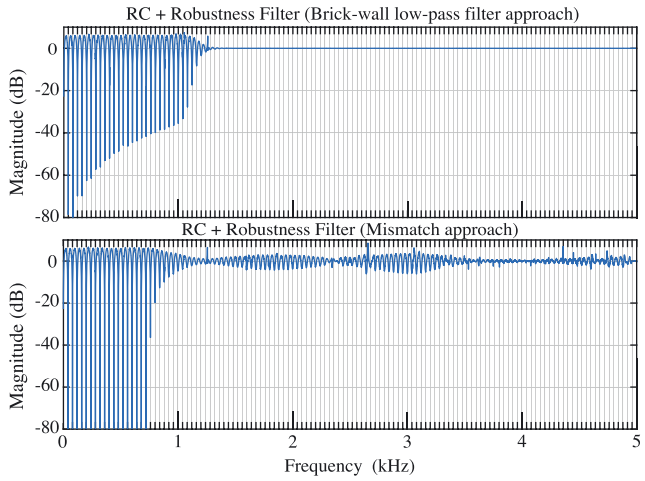

Fig. 13. Sensitivity functions for the two robustness filters.

VII. DISCUSSION

The steady-state tracking error is shown in Fig. 11 and summarized in Tab. I. The results demonstrate a 9% improvement in the ME and 5% for the NRMSE. This improvement is due to increased gain at the majority of signal harmonics.

In Fig. 12, the roll-off rate of the proposed filter can be observed to be slower than the the brick-wall filter. The attenuation of the sensitivity function is also greater at the majority of signal harmonics, as demonstrated in Fig. 13

Note that the robust filter rolls off at a lower frequency than the brick-wall filter. This results in a discrete number of frequencies close to the system bandwidth where the tracking performance of the brick-wall filter could be superior. At these frequencies, the harmonics would be well beyond the system bandwidth so the reference signal would need to be sinusoidal, which is of little practical interest. However, if such conditions were encountered, a weighing function could be added to (47) to control the shape of the over-bound in more detail, making it possible to recover any reduced gain in the resulting robustness filter. In typical applications, the additional complexity of this procedure is not considered to be justified.

The improved attenuation at the harmonic frequencies in the sensitivity function comes at the cost of reduced attenuation between these frequencies. This is due to the restriction imposed by Bode's sensitivity integral [38]. It should be noted, that if the system is subject to significant noise and disturbances for frequencies with reduced sensitivity function attenuation, the performance might deteriorate.

VIII. CONCLUSIONS

A method for improving the performance of repetitive control while preserving robust stability has been described: Convex optimization is used to synthesize the robustness filter from an estimated over-bound of the modeling uncertainty. The result is less conservative than the commonly used brick-wall filter, and the methodology is more automated. Experimental application to a nanopositioning system demonstrated a 9% improvement in the maximum tracking error and a 5% improvement in the root-mean-squared error compared to the traditional approach.

REFERENCES

1. Hara, S., Y. Yamamoto, T. Omata, and M. Nakano, "Repetitive control system: A new type servo system for periodic exogenous signals," *IEEE Trans. Autom. Control*, Vol. 33, No. 7, pp. 659–668 (1988).
2. Francis, B. A. and W. M. Wonham, "Internal model principle of control-theory," *Automatica*, Vol. 12, No. 5, pp. 457–465 (1976).
3. Inoue, T., M. Nakano, T. Kubo, S. Matsumoto, and H. Baba, "High accuracy control of a proton synchrotron magnet power supply," Vol. 20, *Proc. 8th IFAC World Congr.*, pp. 216–221 (1981).
4. Sato, H., T. Sueno, T. Toyama, M. Mikawa, T. Toda, and S. Matsumoto, "High accuracy magnet power supply for proton synchrotron by repetitive control," *Proc. 22nd Annual IEEE Power Electronics Specialists Conf.*, pp. 812–816 (1991).
5. Inoue, T., M. Nakano, and S. Iwai, "High accuracy control of servomechanism for repeated contouring," *Proc. 10th Annual Symp. on Increm. Motion Control Systems and Devices*, Urbana-Champaign, IL, pp. 285–292 (1981).
6. Yamada, M., Z. Riadh, and Y. Funahashi, "Design of discrete-time repetitive control system for pole placement and application," *IEEE/ASME Trans. Mechatron.*, Vol. 4, No. 2, pp. 110–118 (1999).
7. Teo, Y. R. and A. J. Fleming, "A new repetitive control scheme based on non-causal FIR filters," *Proc. Amer. Control Conf.*, Portland, OR, pp. 991–996 (2014).
8. Teo, Y. R., A. A. Eielsen, J. T. Gravdahl, and A. J. Fleming, "Discrete-time repetitive control with model-less FIR filter inversion for high performance nanopositioning," *Proc. IEEE/ASME Int. Conf. on Adv. Intell. Mechatron.*, Besacon, pp. 1664–1669 (2014).
9. Lee, R. C. H. and M. C. Smith, "Repetitive control experiments for a cd player," *Proc. Amer. Control Conf.*, Philadelphia, PA, pp. 2682–2684 (1998).

10. Moon, J., M. Lee, and M. J. Chung, "Repetitive control for the track-following servo system of an optical disk drive," *IEEE Trans. Control Syst. Technol.*, Vol. 6, No. 5, pp. 663–670 (1998).
11. Steinbuch, M., S. Weiland, and T. Singh, "Design of noise and period-time robust high-order repetitive control, with application to optical storage," *Automatica*, Vol. 43, No. 12, pp. 2086–2095 (2007).
12. Kim, D. H. and T. Tsao, "Robust performance control of electrohydraulic actuators for electronic cam motion generation," *IEEE Trans. Control Syst. Technol.*, Vol. 8, No. 2, pp. 220–227 (2000).
13. Escobar, G., P. G. Hernandez-Briones, P. R. Martinez, M. Hernandez-Gomez, and R. E. Torres-Olguin, "A repetitive-based controller for the compensation of $6\ell \pm 1$ harmonic components," *IEEE Trans. Ind. Electron*, Vol. 55, No. 8, pp. 3150–3158 (2008).
14. Fleming, A. J., B. J. Kenton, and K. K. Leang, "Bridging the gap between conventional and video-speed scanning probe microscopes," *Ultramicroscopy*, Vol. 110, No. 9, pp. 1205–1214 (2010).
15. Shan, Y. and K. K. Leang, "Design and control for high-speed nanopositioning: Serial-kinematic nanopositioners and repetitive control for nanofabrication," *IEEE Control Syst. Mag.*, Vol. 33, No. 6, pp. 86–105 (2013).
16. Aridogan, U., Y. Shan, and K. K. Leang, "Design and analysis of discrete-time repetitive control for scanning probe microscopes," *J. Dyn. Syst. Meas. Control -Trans. ASME*, Vol. 131, No. 6, pp. 061103 (12 pages) (2009).
17. Tomizuka, M., T. Tsao, and K. Chew, "Analysis and synthesis of discrete-time repetitive controllers," *J. Dyn. Syst. Meas. Control -Trans. ASME*, Vol. 111, No. 3, pp. 353–358 (1989).
18. Panomruttanarug, B. and R. W. Longman, "Designing optimized FIR repetitive controllers from noisy frequency response data," *Adv. Astronaut. Sci.*, Vol. 127, pp. 1723–1742 (2007).
19. Longman, R. W., "On the theory and design of linear repetitive control systems," *Eur. J. Control.*, Vol. 16, No. 5, pp. 447–496 (2010).
20. Selesnick, I. W., M. Lang, and C. S. Burrus, "Constrained least square design of FIR filters without specified transition bands," *IEEE Trans. Signal Process.*, Vol. 44, No. 8, pp. 1879–1892 (1996).
21. Teo, Y. R., A Eielsen, J. T. Gravdahl, and A. J. Fleming, "A simplified method for discrete-time repetitive control using model-less finite impulse response filter inversion," *J. Dyn. Syst. Meas. Control -Trans. ASME*, Vol. 138, No. 8, pp. 081002 (13 pages) (2016).
22. Rabiner, L. R., "Techniques for designing finite-duration impulse-response digital filters," *IEEE Trans. Commun. Technol.*, Vol. COM-19, No. 2, pp. 188–195 (1971).
23. Inoue, T., "Practical repetitive control system design," *Proc. 29th IEEE Conf. Decis. Contr.*, Honolulu, HI, pp. 1673–1678 (1990).
24. Chew, K.-K. and M. Tomizuka, "Steady-state and stochastic performance of a modified discrete-time prototype repetitive controller," *J. Dyn. Syst. Meas. Control -Trans. ASME*, Vol. 112, No. 1, pp. 35–41 (1990).
25. Yamamoto, Y. and S. Hara, "Internal and external stability and robust stability condition for a class of infinite-dimensional systems," *Automatica*, Vol. 28, No. 1, pp. 81–93 (1992).
26. Yamamoto, Y., "Learning control and related problems in infinite-dimensional systems," In Trentelman, H. L. and J. C. Willems (Eds.) *Essays on control: Perspectives in the theory and its applications*, Birkhäuser, Basel, pp. 191–222 (1993).
27. Pipeleers, G., B. Demeulenaere, J. De Schutter, and J. Swevers, "Robust high-order repetitive control: Optimal performance trade-offs," *Automatica*, Vol. 44, No. 10, pp. 2628–2634 (2008).
28. Hillerstrom, G. and J. Sternby, "Repetitive control using low order models," *Proc. Amer. Control Conf.*, Baltimore, MD, pp. 1873–1878 (1994).
29. Ljung, L., *System Identification: Theory for the User*, 2nd, Prentice Hall, Inc, Upper Saddle River, New Jersey (1999).
30. Welch, P. D., "The use of fast fourier transform for the estimation of power spectra: A method based on time averaging over short, modified periodograms," *IEEE Trans. Audio Electroacoust.*, Vol. 15, No. 2, pp. 70–73 (1967).
31. Osburn, A. W. and M. A. Franchek, "Designing robust repetitive controllers," *J. Dyn. Syst. Meas. Control -Trans. ASME*, Vol. 126, No. 4, pp. 865–872 (2004).
32. Mareels, I. M. Y., M. Gevers, R. R. Bitmead, J. Lygeros, R. L. Kosut, and M. A. Poubelle, "How exciting can a signal really be?," *Syst. Control Lett.*, Vol. 8, No. 3, pp. 197–204 (1987).
33. Rojas, C. R., J. S. Welsh, G. C. Goodwin, and A. Feuer, "Robust optimal experiment design for system identification," *Automatica*, Vol. 43, No. 6, pp. 993–1008 (2007).
34. Grant, M. and S. Boyd, "Graph implementations for nonsmooth convex programs," In Blondel, V, S Boyd, and H Kimura (Eds.) *Recent Advances in Learning and Control*, Lecture Notes in Control and Information Sciences, Springer-Verlag, London, pp. 95–110 (2008).

35. McClellan, J. H., T. W. Parks, and L. R. Rabiner, "A computer program for designing optimum FIR linear phase digital filters," *IEEE Trans. Audio Electroacoust.*, Vol. 21, No. 6, pp. 506–526 (1973).
36. Kenton, B. J. and K. K. Leang, "Design and control of a three-axis serial-kinematic high-bandwidth nanopositioner," *IEEE/ASME Trans. Mechatron.*, Vol. 17, No. 2, pp. 356–369 (2012).
37. Eielsen, A. A., J. T. Gravdahl, and K. K. Leang, "Low-order continuous-time robust repetitive control: Application in nanopositioning," *Mechatronics*, Vol. 30, pp. 231–243 (2015).
38. Goodwin, G. C., S. F. Graebe, and M. E. Salgado, *Control System Design*, Prentice Hall, Upper Saddle, River, NJ (2000).

Arnfinn A. Eielsen was born in Stavanger, Norway in 1980. He received the siv.ing. (MSc) degree and the Ph.D. degree in Engineering Cybernetics from the Department of Engineering Cybernetics, at the Norwegian University of Science and Technology (NTNU), Trondheim, Norway in 2007 and 2012, respectively. During his doctoral studies he was a visiting academic at the University of Nevada, Reno, and the University of Newcastle (UoN), Australia. After the completion of the Ph.D degree he was a Postdoctoral Research Fellow at the Department of Engineering Cybernetics at NTNU, focusing on motion control and instrumentation. He is currently employed as a Research Fellow in the School of Electrical Engineering and Computer Science at UoN. Research interests include mathematical modeling, identification, adaptive systems, motion control, and control theory in general. He is a member of IEEE.

Yik R. Teo graduated from The University of Newcastle, Australia (Callaghan campus) with a Bachelor of Electrical Engineering (1st Class Honors) in 2010 and a Master of Philosophy in Mechanical Engineering in 2013. He is currently pursuing his Ph.D. under the supervision of Dr. Andrew J Fleming at the Precision Mechatronics Lab located at The University of Newcastle, Australia. His research includes high-precision positioning, scanning probe microscopy, and nano-fabrication. Academic awards include the Glenn and Ken Moss Research Higher Degree Award, Australian Postgraduate Award and the Vice-Chancellor Award in Outstanding Research Candidate.

Andrew J. Fleming graduated from The University of Newcastle, Australia (Callaghan campus) with a Bachelor of Electrical Engineering in 2000 and Ph.D in 2004. Dr. Fleming is presently an Australian Research Council Future Fellow and Director of the Precision Mechatronics Lab at The University of Newcastle, Australia. His research interests include biomedical devices, lithography, nano-positioning, and scanning probe microscopy. Dr. Fleming's research awards include the IEEE Transactions on Control Systems Technology Outstanding Paper Award and The University of Newcastle Researcher of the Year Award. He is the co-author of three books and more than 150 Journal and Conference articles. Dr. Fleming is the inventor of several patent applications, and in 2012 he received the Newcastle Innovation Rising Star Award for Excellence in Industrial Engagement.